NASA TECHNICAL MEMORANDUM

NASA TM X-1781

NASA TM X-1781

FORCES ON A FLEXIBLE SHELL DURING WATER IMPACT

by David A. Hamilton

Manned Spacecraft Center
Houston, Texas

NATIONAL AERONAUTICS AND SPACE ADMINISTRATION • WASHINGTON, D. C. • MAY 1969

NASA TM X-1781

FORCES ON A FLEXIBLE SHELL DURING WATER IMPACT

By David A. Hamilton

Manned Spacecraft Center
Houston, Texas

NATIONAL AERONAUTICS AND SPACE ADMINISTRATION

For sale by the Clearinghouse for Federal Scientific and Technical Information
Springfield, Virginia 22151 – CFSTI price $3.00

ABSTRACT

Water impact tests were conducted with a 1/4-scale model of the Apollo command module. The tests were made to observe loads on the heat shield and at the center of gravity of the model. Results showed the nature of the loading on the center of gravity and related the loading to the heat-shield accelerations and the water-pressure force.

FORCES ON A FLEXIBLE SHELL DURING WATER IMPACT

By David A. Hamilton
Manned Spacecraft Center

SUMMARY

An experimental investigation was conducted to observe the structural loads produced during water impact of a 1/4-scale model of the Apollo command module. The heat shield of the model was scaled elastically from an early Apollo heat-shield design that had a symmetric thickness.

The model was tested at full-scale vertical velocities that ranged from 16 to 25 fps and at zero horizontal velocity. Pitch angles were varied from 0° to 20° with primary emphasis at 0°.

Test results were indicative that the flexible heat-shield model experienced impact loads on the structure which were up to twice as great as experienced by a rigid shell of the same geometry and weight under the same impact conditions. Maximum impact loads occurred at a pitch angle of 0° and decreased to near rigid-shell loads at pitch angles of approximately 15°. This report contains an analysis of the higher impact loads on the flexible heat shield and the center of gravity of the model.

INTRODUCTION

Water is the primary landing medium for the Apollo command module (CM). Therefore, the effect of water impact upon the spacecraft structure has been the subject of much investigation.

Data on water impact have been gathered from seaplane research. The water-impact analysis by Von Kármán, discussed in appendix A, has been used to predict seaplane loads during water impact. Seaplane research has resulted in concepts that are applicable to water impact of a rigid shell. However, the Apollo CM has a flexible heat shield that may experience higher loads during impact than are experienced by a rigid shell of the same geometry and weight. Therefore, rigid-shell theory is not directly applicable to the Apollo CM.

Because a method for predicting impact loads for the Apollo CM was needed, Langley Research Center (LRC) devoted extensive research to comparing Apollo CM models that had either rigid or flexible heat shields. Good correlation was established

between a modified Von Kármán analysis and the results of rigid heat-shield experiments at LRC.

It is the objective of this report to show that the higher impact forces experienced by the flexible heat-shield model during water impact exist not only at the center of gravity (c.g.) of the model but also on the heat shield.

SYMBOLS

A	area
a	acceleration
d	radial distance along deflecting diameter of heat shield from a fixed reference point
F	force
F_r	upper-body response force
F_w	water-pressure force
I	moment of inertia
L	radial deflecting diameter of heat shield
M	momentum
m	mass
m_1	effective heat-shield mass
m_b	body mass
m_v	virtual mass
P	pressure
R	radius of sphere
S	length of wedge
t	time
V	volume

v	velocity
v_h	horizontal velocity
v_o	impact velocity
v_t	velocity at time t after impact
v_v	vertical velocity
W	weight
$X_{1,R}$	deflection of heat-shield center relative to upper body
$\dot{X}_{1,R}$	velocity of heat-shield center relative to upper body
$\ddot{X}_1$	acceleration of heat-shield center
$\ddot{X}_{1,R}$	acceleration of heat-shield center relative to upper body
$\ddot{X}_2$	upper-body acceleration
$\overline{X}_1$	average heat-shield displacement
$\overline{X}_{1,R}$	average heat-shield deflection relative to upper body
$\overline{\dot{X}}_{1,R}$	average heat-shield velocity relative to upper body
$\overline{\ddot{X}}_1$	average heat-shield acceleration
$\overline{\ddot{X}}_{1,R}$	average heat-shield acceleration relative to upper body
Y	one-half width of wedge at water surface
y	scale of model
Z	penetration of sphere
β	variable of trigonometric function
θ	angle between wedge side and water surface

ρ density of water

ϕ pitch angle

MODEL DESCRIPTION

The experimental model consisted of a 1/4-scale dynamically modeled heat shield attached to a rigid upper body. Sectional views of the model are shown in figure 1, and model and full-scale relationships are presented in table I.

The heat shield was attached to the body by wood screws on a bolt-circle pattern located at a position scaled to the position of the bolt circle on the full-scale CM. The upper body was constructed of laminated plywood cut to heat-shield curvature at the surface of contact with the heat shield. The location of the center of gravity is shown in figure 1, and the moments of inertia and model dimensions are given in table II. The model inertias were not scaled properly to the full-scale Apollo CM, but little effect on impact loads resulted, because angular accelerations were small at low pitch angles.

The heat-shield stiffness was scaled to an early Apollo design, but failure strength was not scaled. The sandwich construction of the heat shield (fig. 2) consisted of a core of styrene plastic covered on each side by two layers of glass cloth that were impregnated with epoxy resin. A uniaxial aluminum accelerometer mount was bonded on the inner surface of the heat shield with epoxy, and a triaxial mount was bolted to the upper body. The heat-shield accelerometer was mounted in the X direction, and the upper-body accelerometers were mounted in the X, Y, and Z directions.

APPARATUS AND PROCEDURE

Test Conditions

The model test series consisted of vertical drops into water at velocities ranging from 8 to 12.5 fps, which correspond to 16 to 25 fps full scale. The full-scale velocities were not as great as actual Apollo impact velocities but were sufficient to demonstrate the effect of heat-shield flexibility upon impact loads. Pitch angles were varied from 0° to 20° (fig. 3), with primary emphasis on the pitch angle of 0°.

Launch Apparatus

The launch-release mechanism was a U.S. Air Force bomb release. All drops were vertical, and height was adjusted to produce the desired impact velocity from free fall.

Instrumentation

Accelerations were measured (with strain-gage accelerometers) at the center of gravity and on the heat shield of the model. The response characteristics of the accelerometers are presented in table III. A digital programer automatically controlled both the data-recording system and the release mechanism. An oscillograph was used to record acceleration data.

DISCUSSION

Structural design criteria for water impact of the Apollo CM were based on the assumption that loads on a flexible heat shield during water impact would not exceed loads experienced by a rigid body of the same geometry and weight. In subsequent research at LRC on Apollo CM models with flexible heat shields, it was established that the flexible heat-shield models could experience center-of-gravity accelerations as great as twice the accelerations on a rigid heat-shield model. Research was conducted at the Manned Spacecraft Center (MSC) to analyze further the effect of the heat-shield structural oscillations that affect impact forces on the heat shield and accelerations at the model center of gravity.

Typical test data for the 1/4-scale Apollo CM model used in the MSC test program are shown in figure 4. Center-of-gravity accelerations for models with both flexible and rigid heat shields are given in figures 5 and 6. The comparison of rigid- and flexible-shell center-of-gravity accelerations indicate that the flexible heat-shield model experiences significantly higher accelerations under the same impact conditions.

Oscillations of the flexible heat shield are the primary reason for the difference in flexible- and rigid-body impact loads. The amplitudes of the heat-shield oscillations are small compared with heat-shield radius of curvature (heat-shield radius is 44 inches, heat-shield deflection is less than 0.5 inch), but the effect on impact loads is significant.

To illustrate the effect of the inertia load produced by the oscillations of the flexible heat shield, it is convenient to represent the heat shield and the upper body by a simple spring-mass system (fig. 7). An effective heat-shield mass is assumed that corresponds to the part of the heat shield which is deflected during impact. The acceleration of this effective mass is calculated by the use of an assumed deflection shape. As illustrated in figure 8, the cross-sectional deflected shape of the heat shield is assumed to correspond to the shape of a $(1 - \cos 2\pi d/L)$ curve, where L is a fixed distance. The effective mass and deflected shape assumptions are based on data from a series of accelerometers across the heat shield which give an indication of the relative deflections of the heat shield at various locations. A relationship is established (by the deflected shape) between the maximum relative heat-shield deflection and the relative deflection of any other point on the deflecting surface. During one period of a $(1 - \cos \beta)$ curve, the average amplitude is one-half the maximum amplitude. This relationship is applicable to the deflecting heat shield because the average relative deflection $\bar{X}_{1,R}$ is one-half the relative deflection of the heat-shield

center $X_{1,R}$ at any time for a vertical impact at a pitch of 0°. This expression is written

$$\overline{X}_{1,R} = 0.50\, X_{1,R} \tag{1}$$

and the same relationship exists between maximum and average values of relative velocity and acceleration, as shown in equations (2) and (3).

$$\overline{\dot{X}}_{1,R} = 0.50\, \dot{X}_{1,R} \tag{2}$$

$$\overline{\ddot{X}}_{1,R} = 0.50\, \ddot{X}_{1,R} \tag{3}$$

The acceleration of the heat-shield center $\ddot{X}_1$ minus the upper-body acceleration $\ddot{X}_2$ by definition gives the relative acceleration between the two values.

$$\ddot{X}_{1,R} = \ddot{X}_1 - \ddot{X}_2 \tag{4}$$

Calculation of $\ddot{X}_{1,R}$ for specific impact conditions is given in figure 9. Equations (3) and (4) can be combined to establish a relationship between average relative heat-shield acceleration and the impact data $\ddot{X}_1$ and $\ddot{X}_2$.

$$\overline{\ddot{X}}_{1,R} = 0.50\left(\ddot{X}_1 - \ddot{X}_2\right) \tag{5}$$

Because $\overline{\ddot{X}}_{1,R}$ is the average relative acceleration, $\overline{\ddot{X}}_{1,R}$ can be combined with $\ddot{X}_2$ to define the average heat-shield acceleration

$$\overline{\ddot{X}}_1 = \overline{\ddot{X}}_{1,R} + \ddot{X}_2 \tag{6}$$

This acceleration (fig. 10) of the effective heat-shield mass can be used with the effective mass to determine the inertia force of the heat shield during impact.

For the spring-mass system shown in figure 7, the governing equation is

$$F_w = m_1\ddot{\bar{X}}_1 + m_b\ddot{X}_2 \tag{7}$$

where m_1 is the effective heat-shield mass and m_b is the body mass. The calculated water-pressure force F_w is plotted in figure 11 for a specific test. The comparison of $m_1\ddot{\bar{X}}_1$ and F_w in figure 11 shows that the heat-shield inertia load is small relative to the water-pressure force and the upper-body inertia force. The water-pressure force corresponds closely to the upper-body response force $m_b\ddot{X}_2$, as shown in figure 11. This correlation of forces means that the higher loads of the flexible heat-shield model exist not only at the center of gravity of the model but also on the heat shield. Similar results were obtained from a recent experimental investigation conducted at LRC utilizing pressure measurements on the heat-shield surface (ref. 1).

The velocity of the flexible heat shield varies significantly from the velocity of the rigid shell under the same impact conditions. The acceleration of the flexible heat-shield center for a specific test is presented in figure 12. This acceleration can be integrated with respect to time to determine the velocity of the heat-shield center at any time. The velocity decay of the heat-shield center and the rigid shell under the same impact conditions are compared in figure 13. This variation of velocity violates the momentum equation (ref. 2)

$$m_b v_o = (m_b + m_v) v_t \tag{8}$$

(where v_o is impact velocity, m_v is the associated or virtual mass, and v_t is the velocity at time t after impact) which Von Kármán developed to define forces on a wedge during water impact. There is no single velocity v_t for the heat shield, the virtual mass, and the upper body. If a momentum equation is to be developed to define forces on a flexible shell during impact, the equation must be a function of heat shield, virtual mass, and upper-body velocities and the corresponding masses.

As noted previously, impact loads are highest at a pitch angle of 0° and decrease to near rigid-body loads at pitch angles of approximately 15°. A plot of X-axis acceleration versus pitch angle is given in figure 14. As the pitch angle increases, a smaller impact load is experienced as a result of a decrease in the amplitude of structural oscillations of the flexible heat shield. At pitch angles greater than 15°, the wetted area extends beyond the edge of the heat shield before the time of maximum impact force, so that the sphere-impact analysis is no longer valid.

CONCLUDING REMARKS

The data for the flexible heat-shield model were indicative that impact loads were experienced up to twice the loads on a rigid shell with the same impact conditions. The inertia load of the heat shield (produced by the oscillations) is small compared with the upper-body response force and the water-pressure force. The water-pressure force is approximately equal in magnitude and frequency to the body response force. Thus, it may be noted that the higher loads of the flexible body exist not only at the center of gravity of the model but also on the heat shield.

Manned Spacecraft Center
National Aeronautics and Space Administration
Houston, Texas, February 28, 1969
914-11-20-17-72

TABLE I. - SCALE RELATIONSHIP (EARTH)

[y = scale of model]

Quantity	Full size	Scale factor	Model
Length	d	y	yd
Area	A	y^2	y^2A
Volume	V	y^3	y^3V
Weight	w	y^3	y^3w
Time	t	$\sqrt{y}$	$\sqrt{y}\,t$
Velocity	v	$\sqrt{y}$	$\sqrt{y}\,v$
Acceleration	a	1	a
Mass	m	y^3	y^3m
Momentum	M	$y^{3.5}$	$y^{3.5}M$
Moment of inertia	I	y^5	y^5I
Force	F	y^3	y^3F
Pressure	P	y	yP

TABLE II. - MODEL AND FULL-SCALE PARAMETERS

Mass, slugs	Moments of inertia, slug-ft^2			Dimensions, in.		
	Roll	Pitch	Yaw	Diameter	Height	Spherical radius of heat shield
1/4-scale model*						
6.02	5.83	3.85	3.85	37.88	15.50	44.15
Full-scale vehicle						
280	4340	3680	3080	151.50	84.84	176.60

*Only heat-shield diameter and spherical radius are scaled according to the scale relationship in table I.

TABLE III. - INSTRUMENTATION CHARACTERISTICS

Accelerometer orientation	Normal (c.g.)	Normal (heat shield)	Longitudinal (c.g.)
Range, g	±50	±50	±25
Natural frequency, Hz	900	900	900
Damping, percent of critical damping	60	60	60
Limiting system response frequency, Hz	600	600	600

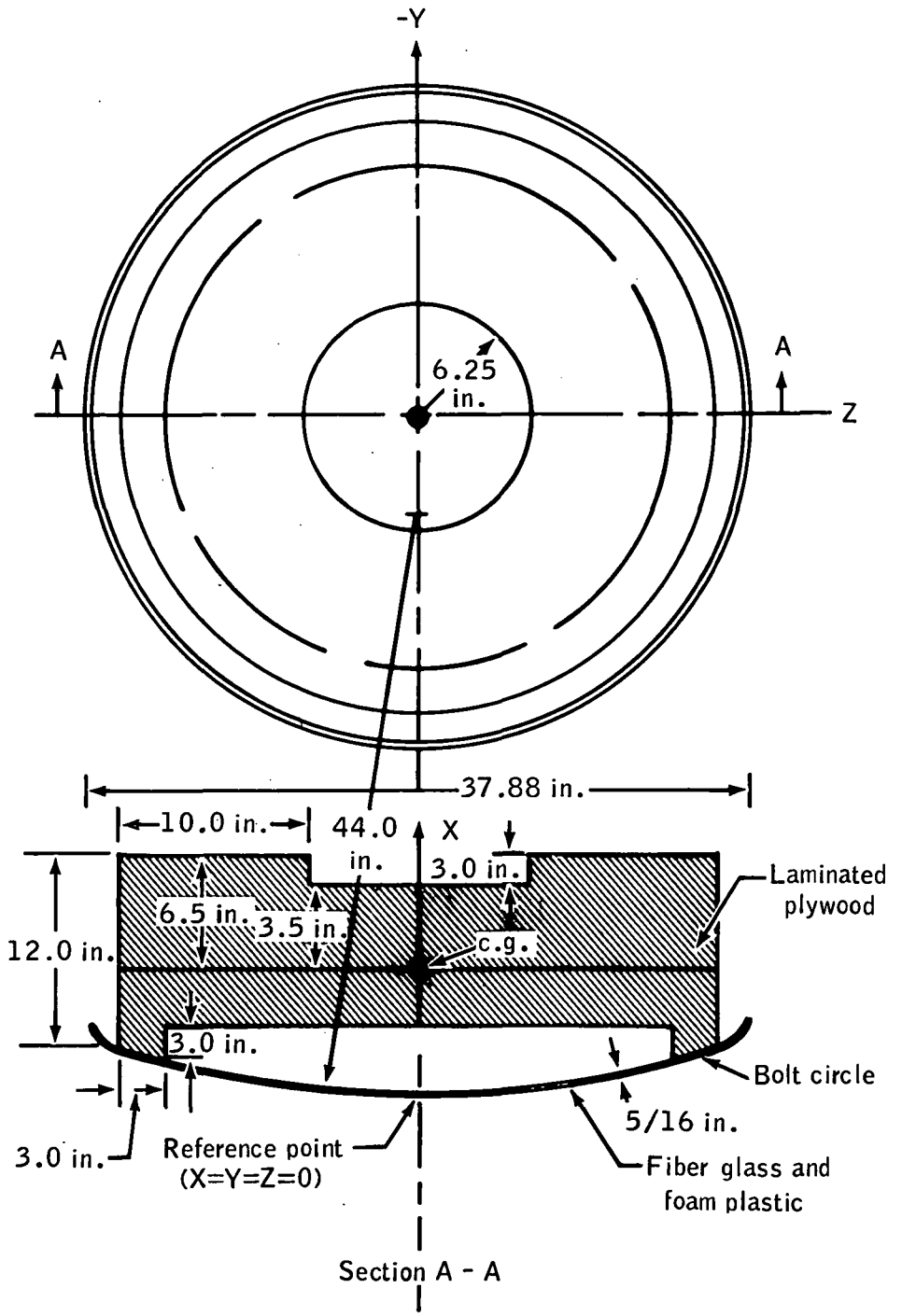

Figure 1. - Model dimensions and characteristics.

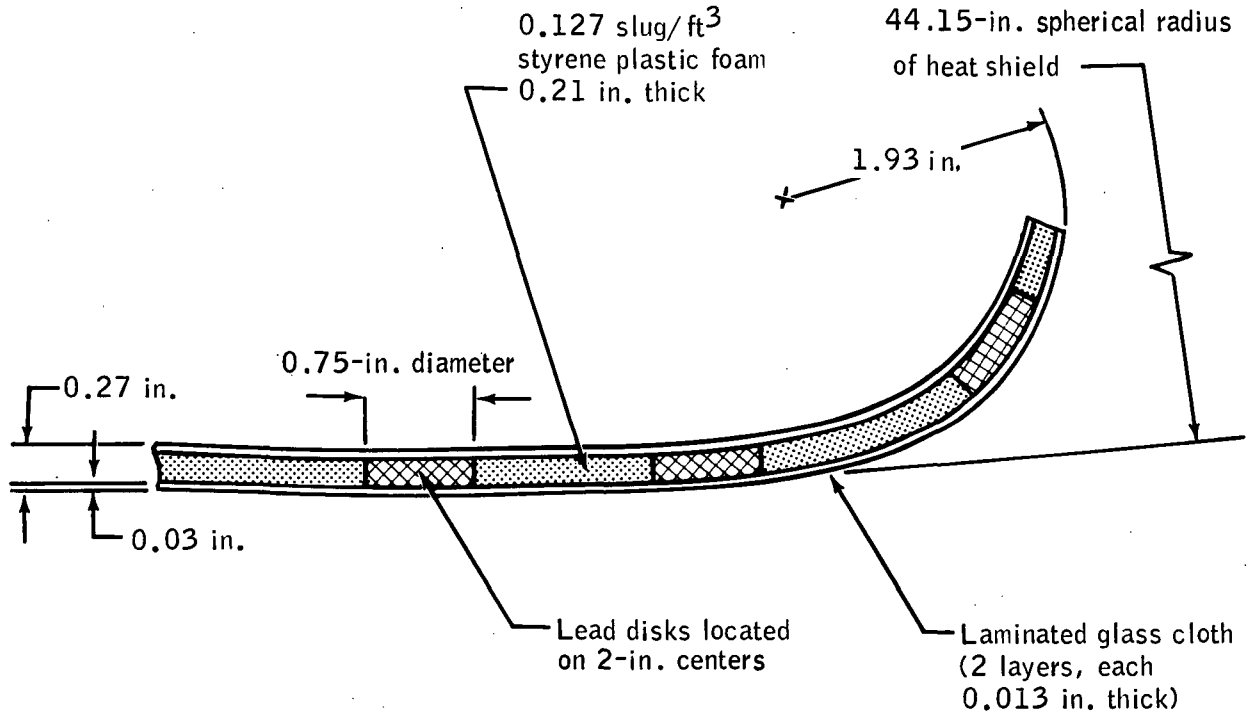

Figure 2. - Heat-shield construction details (model values).

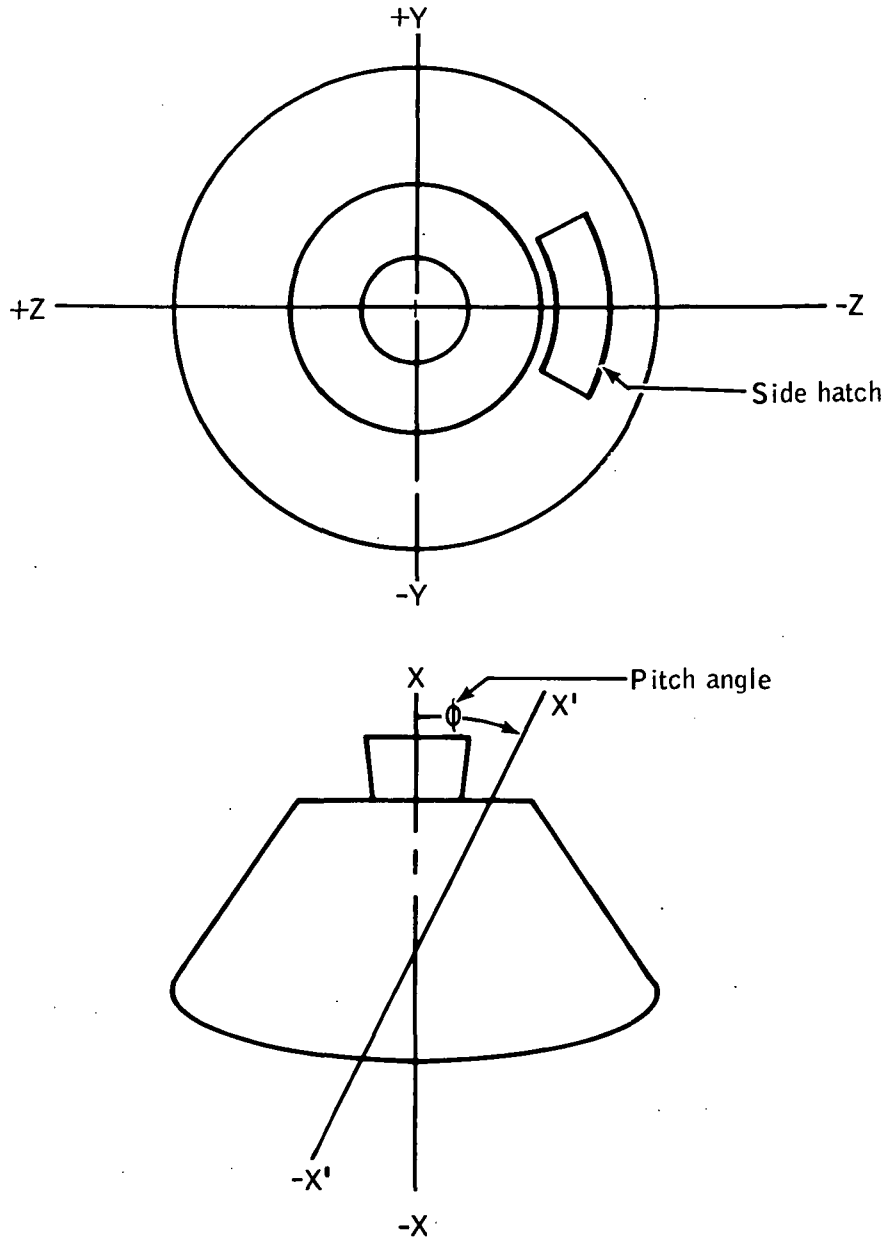

Figure 3. - Apollo command-module axis orientation.

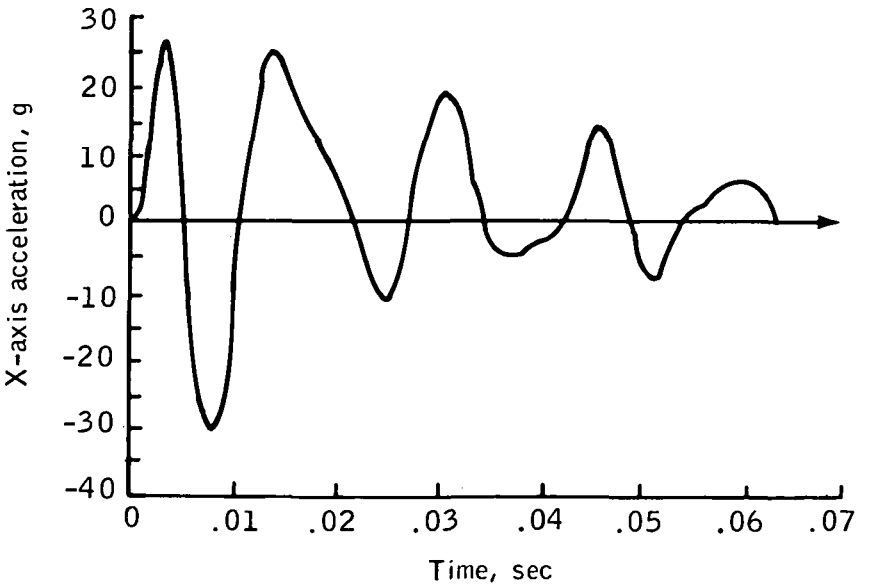

(a) Heat-shield center.

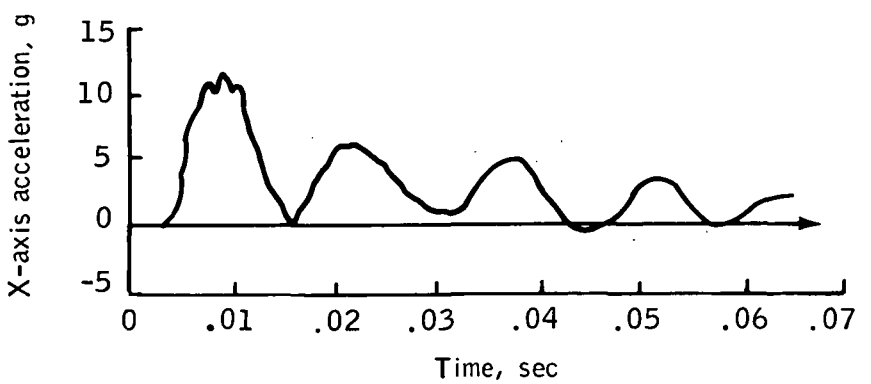

(b) Center of gravity.

Figure 4. - Typical acceleration data.

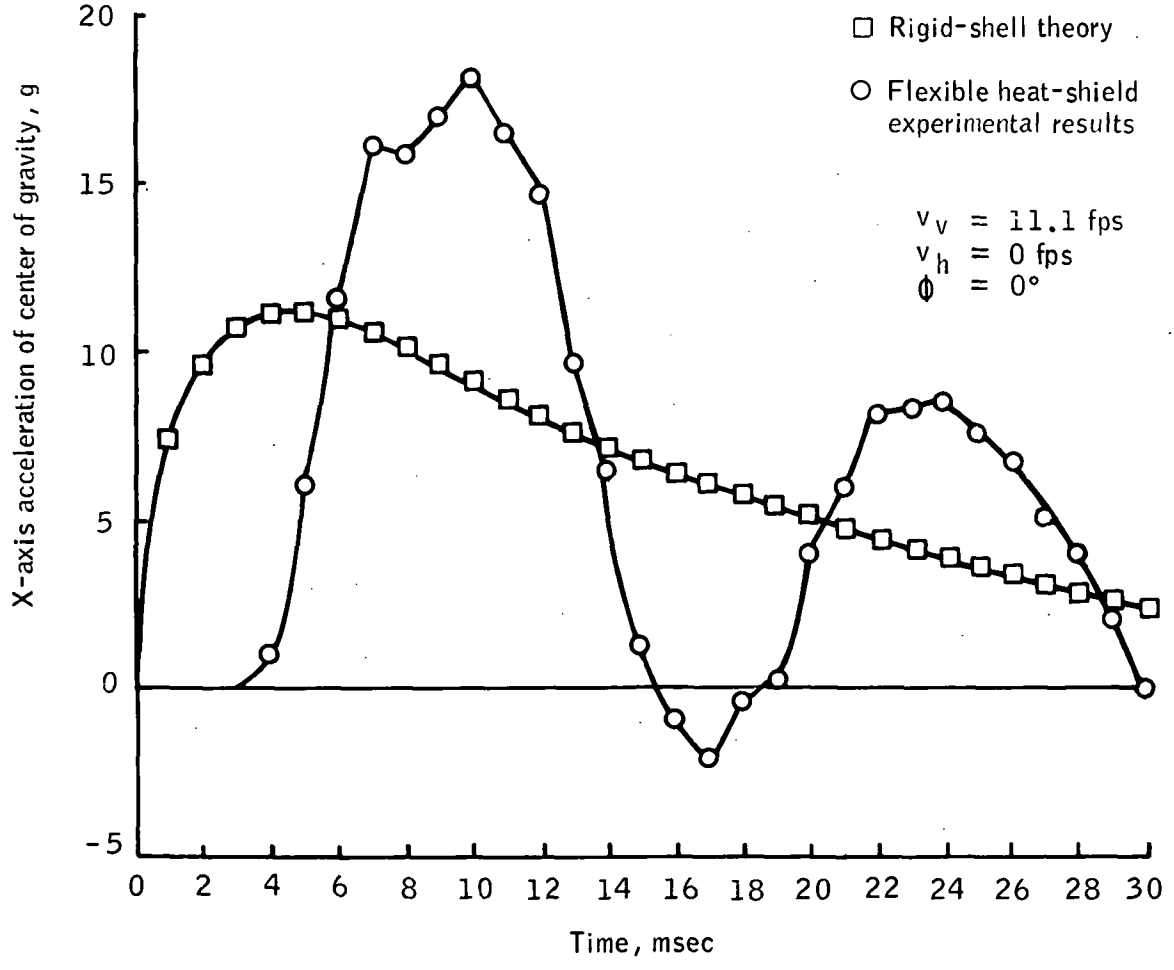

Figure 5. - Comparison of flexible and rigid heat-shield impact acceleration at center of gravity (V_v = 11.1 fps).

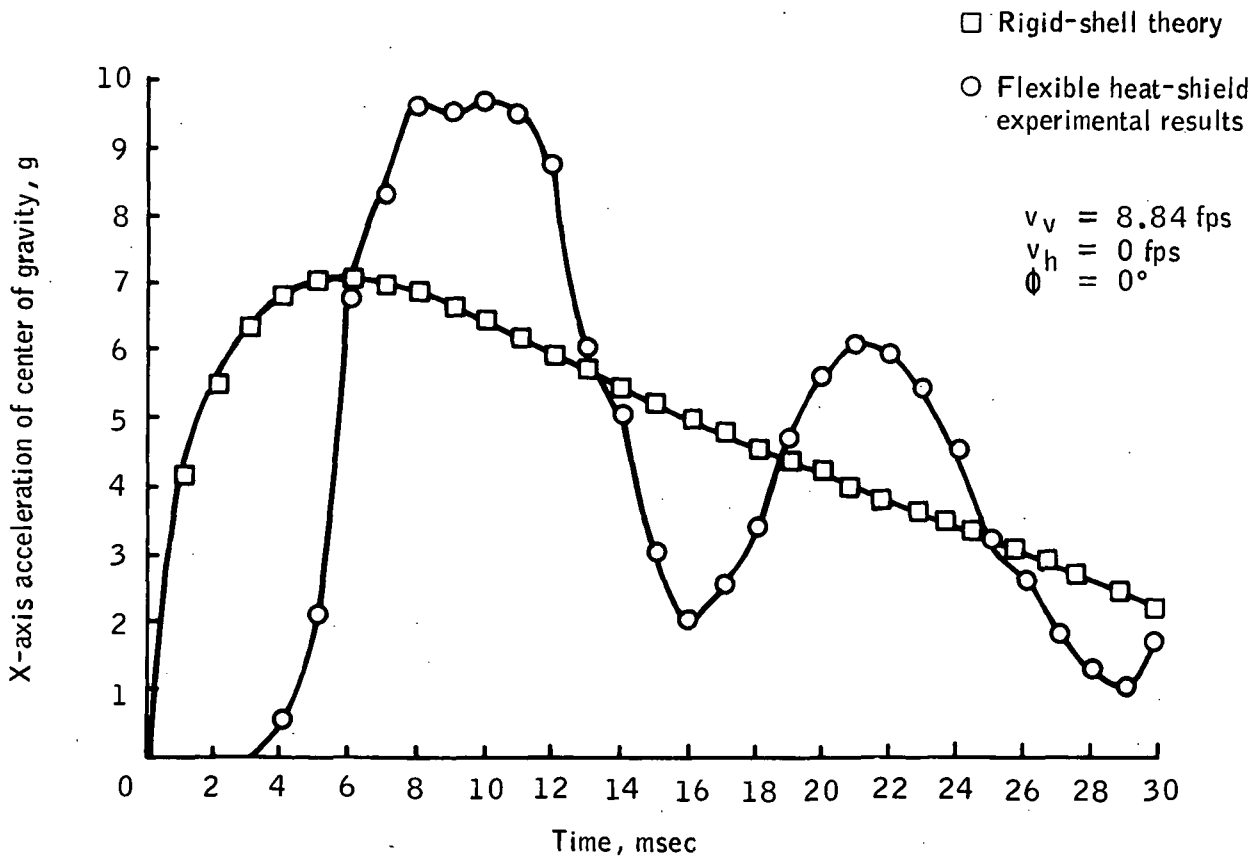

Figure 6. - Comparison of flexible and rigid heat-shield impact acceleration at center of gravity (V_v = 8.84 fps).

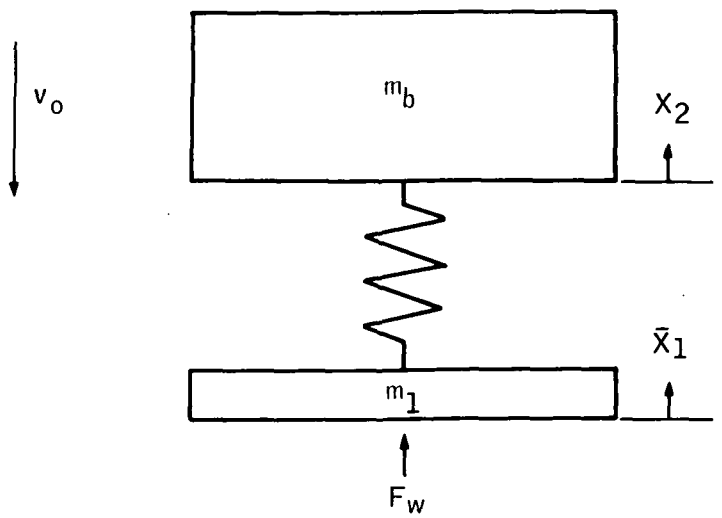

(a) Simple spring-mass system.

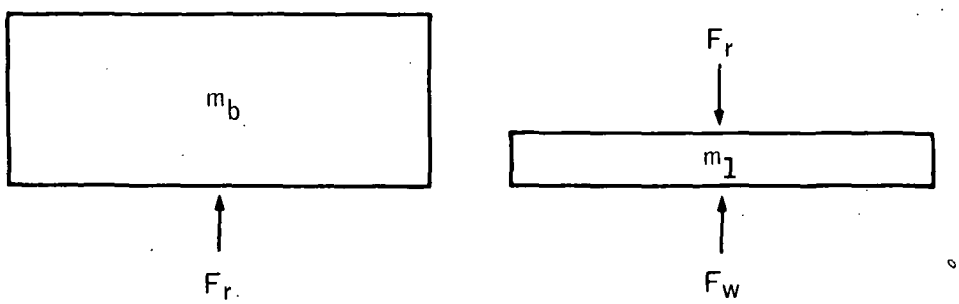

Differential equation:

$$m_b \ddot{X}_2 = F_r$$

Differential equation:

$$m_1 \ddot{\bar{X}}_1 = F_w - F_r$$

(b) Free-body diagrams.

Figure 7. - Simple spring-mass system subjected to a force, and the corresponding free-body diagrams.

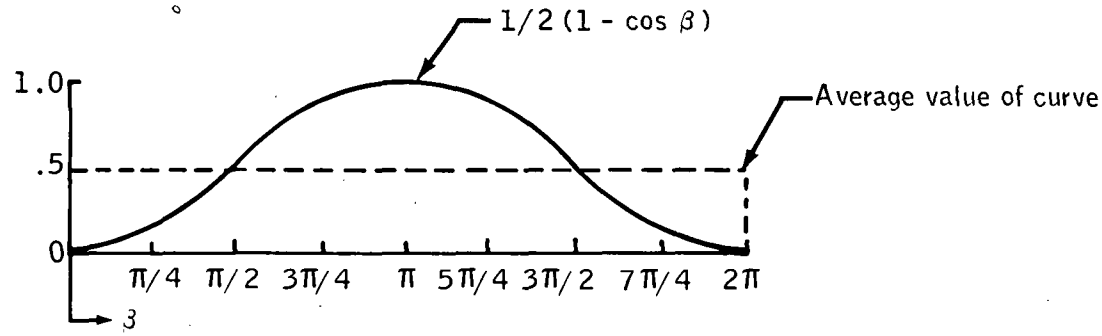

(a) The 1/2 (1 - cos β) curve.

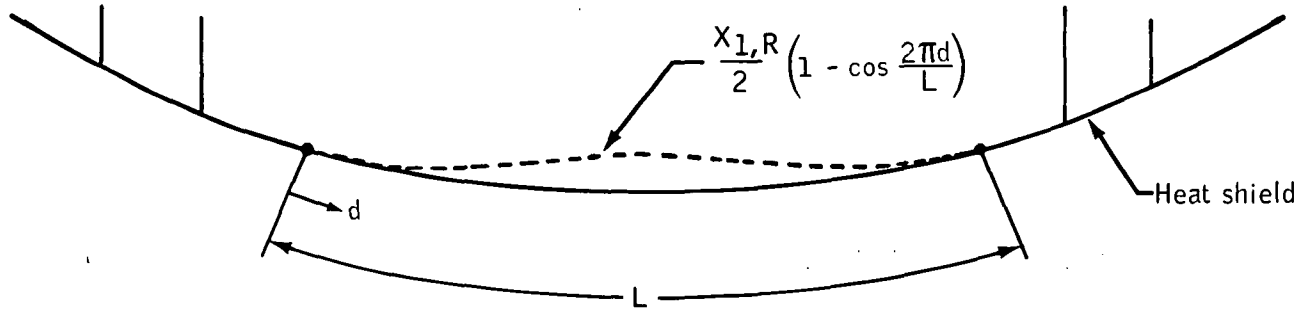

(b) Heat-shield deflection.

Figure 8. - Assumed deflection shape of heat shield.

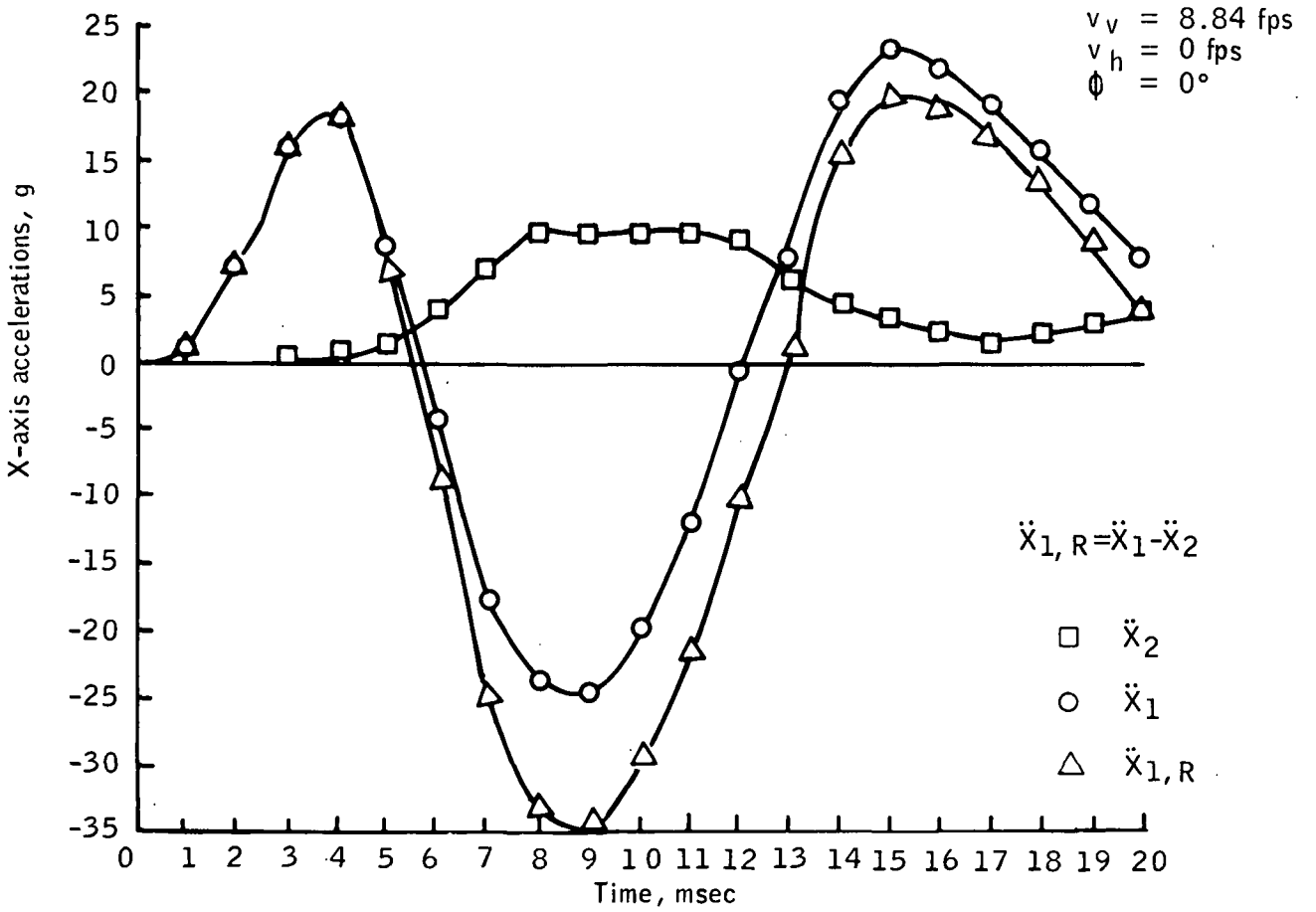

Figure 9. - X-axis accelerations of heat-shield center, upper body, and heat-shield center relative to upper body.

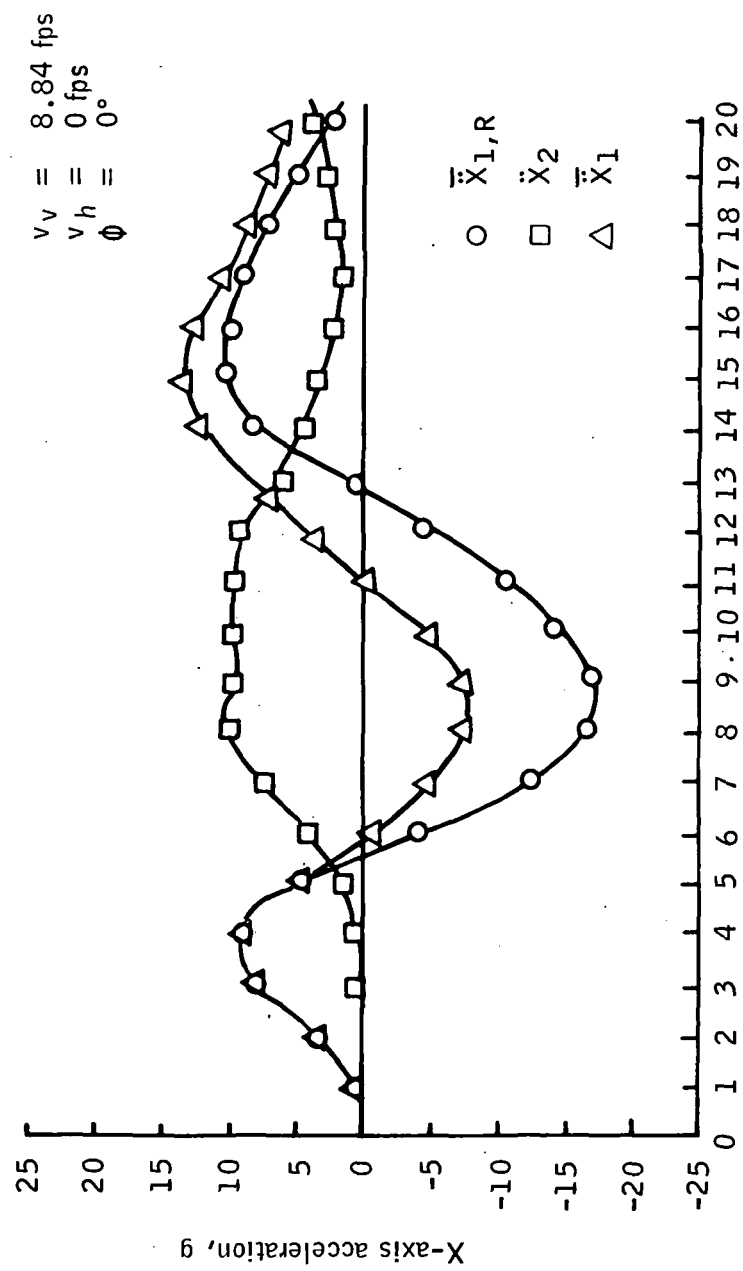

Figure 10. - Average relative acceleration of heat shield, average acceleration of heat shield, and upper-body acceleration.

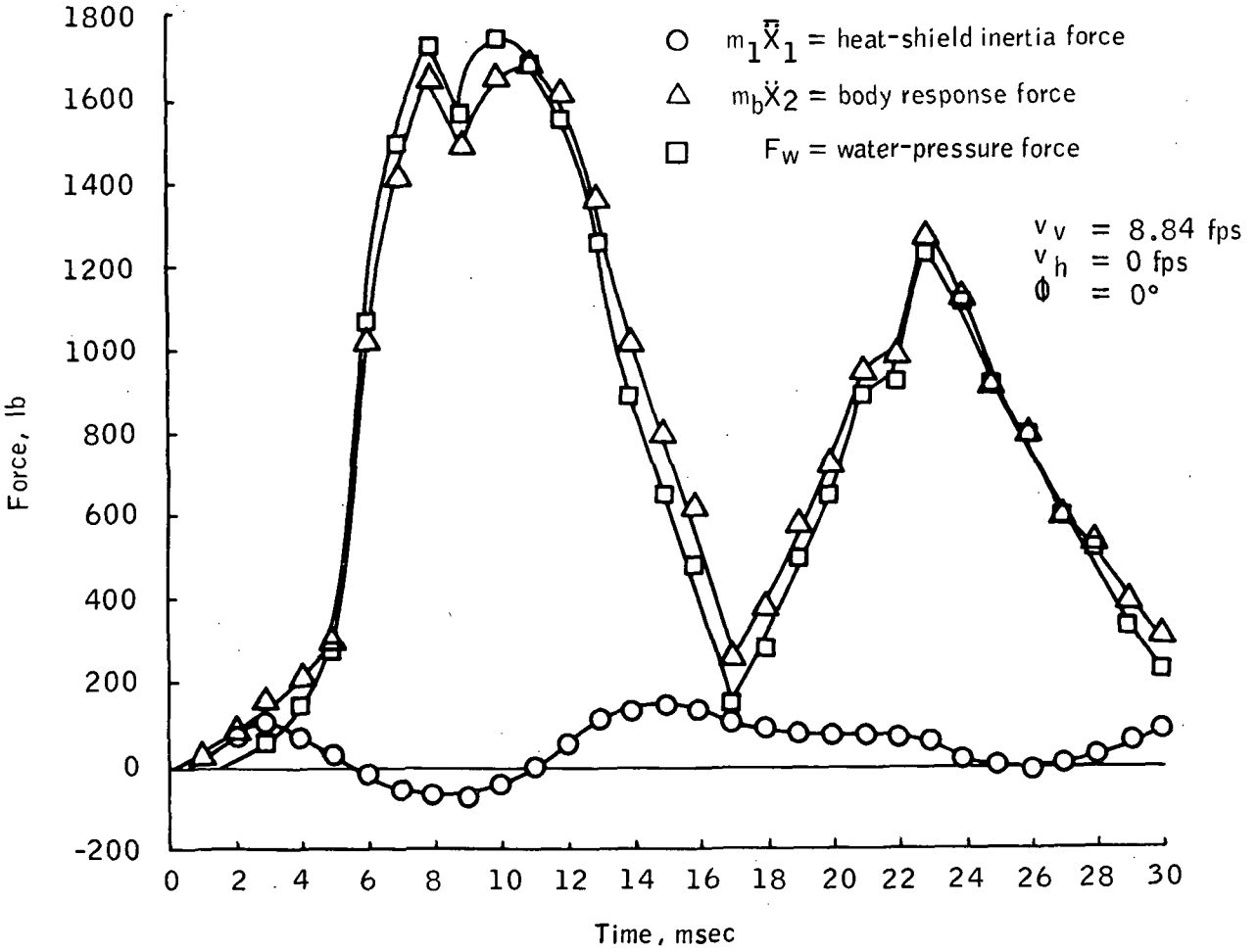

Figure 11. - Inertia forces of heat shield and upper body, and water-pressure force.

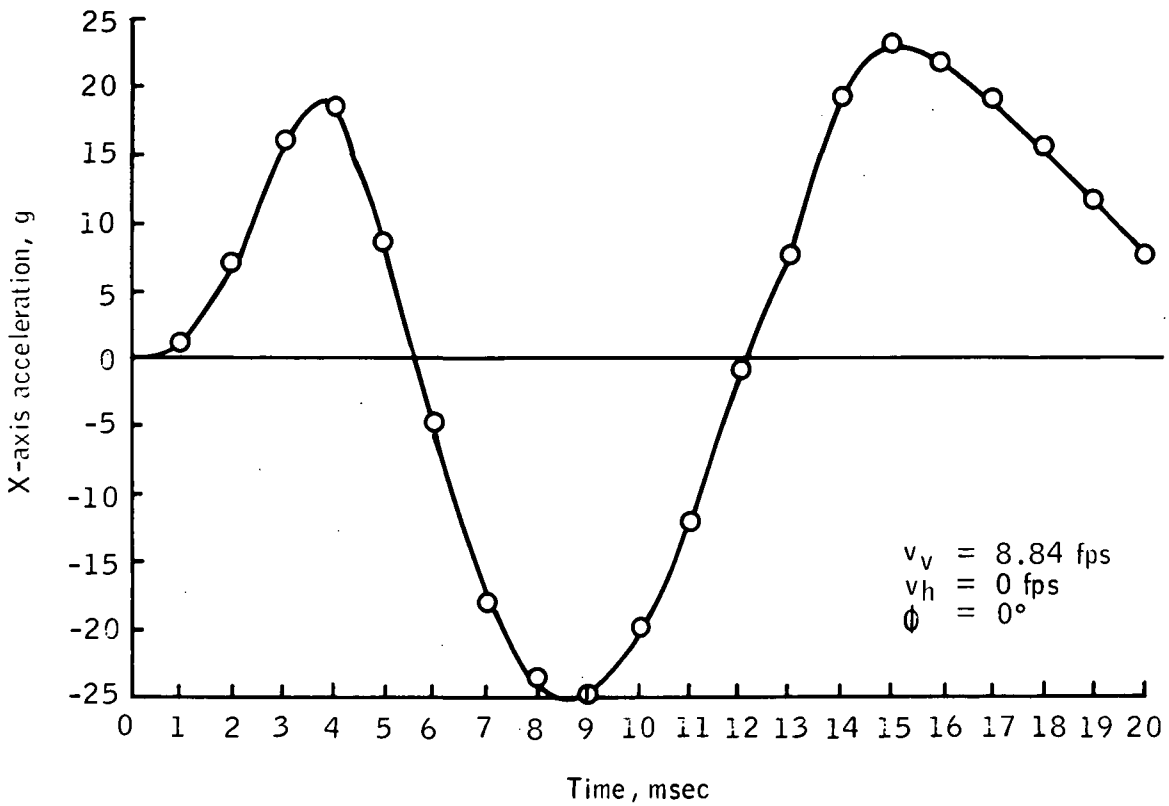

Figure 12. - Acceleration-time history of the heat-shield center.

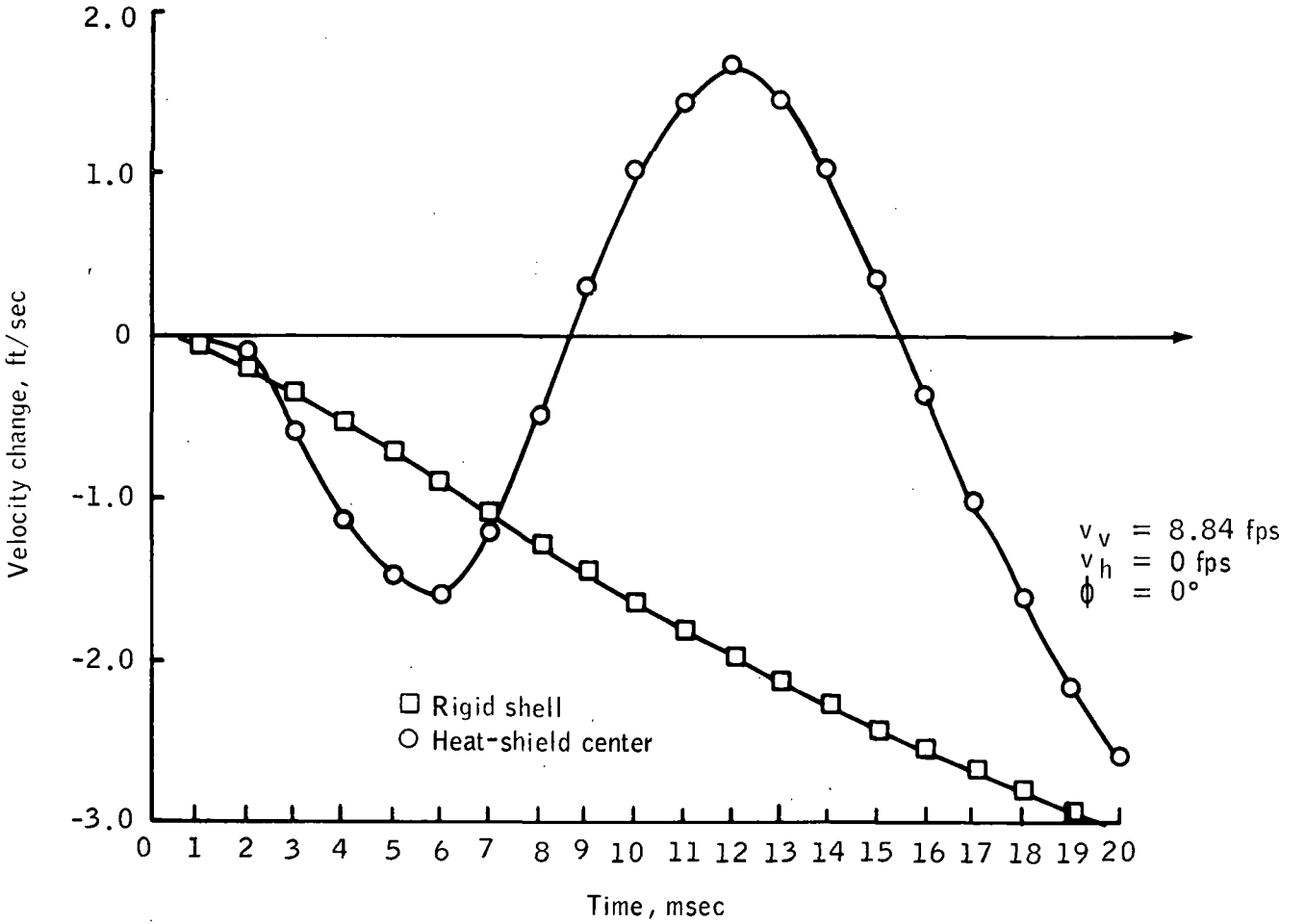

Figure 13. - Comparison of velocity change after impact for rigid shell and heat-shield center.

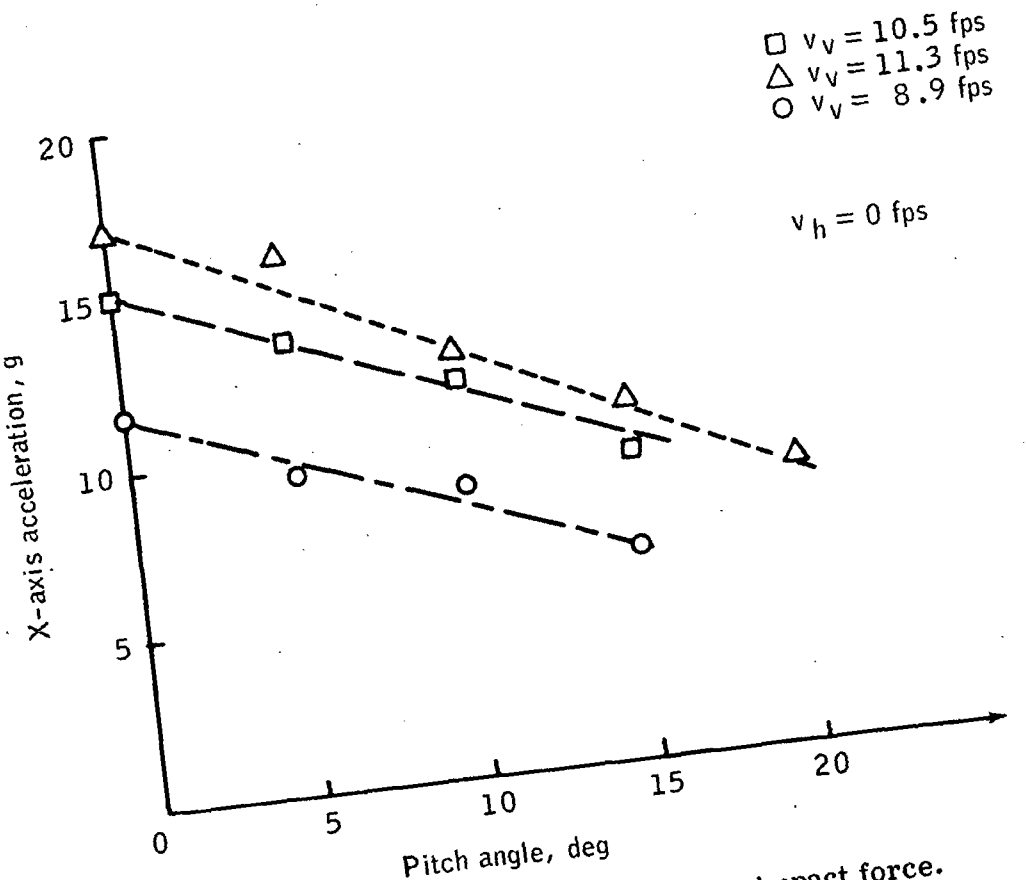

Figure 14.- Effect of pitch angle on impact force.

APPENDIX A

VON KÁRMÁN ANALYSIS OF WEDGE IMPACT

Von Kármán considered the vertical impact of a wedge-shaped body into a horizontal water surface as shown in figure A-1. The basis of this theory is that the vertical momentum of the wedge before impact is imparted both to the wedge and to an associated mass of water after initial impact. This statement is expressed mathematically as equation (8). Von Kármán pointed out that the virtual mass is equal to the mass of a semicylinder of water having a diameter equal to the width of the wedge in water and a length equal to the length of the wedge. The assumption of a semicylinder of water is only a convenient tool which gives a good approximation of an average mass of water which moves at the velocity of the body.

As developed in reference 3, development of equation (8) leads to the impact force equation for a wedge, which is

$$F = \frac{-\pi\rho SY v_o^2 \cot\theta}{\left(1 + \frac{\pi\rho SY^2}{2m}\right)^3} \tag{A1}$$

where ρ is the density of water, S is the wedge length, Y is one-half the width of the wedge at the water surface, and θ is the angle between the wedge side and the water surface.

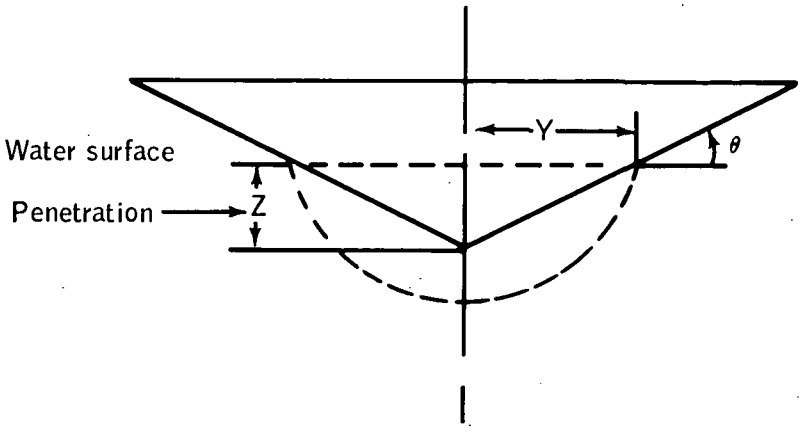

Figure A-1. - Geometry of wedge at water impact.

APPENDIX B

VON KÁRMÁN WATER IMPACT ANALYSIS MODIFIED FOR A SPHERE

To apply the Von Kármán analysis to the shape of the Apollo heat shield, it is necessary first to develop relationships for the impact of a sphere on water. Analogous to the wedge impact, the virtual mass for a sphere impacting water is equal to a hemisphere of water the diameter of which is equal to the width of the sphere in water as shown in figure B-1. The virtual mass is

$$m_v = \frac{2}{3}\rho\pi\left(2RZ - Z^2\right)^{3/2} \tag{B1}$$

where R is the radius of the sphere and Z is the penetration.

Extensive LRC studies (ref. 4) of Apollo rigid heat-shield models proved that the virtual mass that best predicted experimental results was actually 0.9 times the mass of a hemisphere of water the diameter of which equals the width of the sphere in water. Therefore, for the Apollo models

$$m_v = 0.9\left[\frac{2}{3}\rho\pi\left(2RZ - Z^2\right)^{3/2}\right] \tag{B2}$$

or

$$m_v = 0.6\rho\pi\left(2RZ - Z^2\right)^{3/2} \tag{B3}$$

The momentum equation for this case becomes

$$m_b v_o = m_b v_t + \left[0.6\rho\pi\left(2RZ - Z^2\right)^{3/2}\right] v_t \tag{B4}$$

Following a similar development, as in reference 3, the impact force on the Apollo CM at vertical impact is

$$F = \frac{-0.9 v_t^2 \rho\pi \left(2RZ - Z^2\right)^{1/2} (2R - 2Z)}{1 + \frac{3\rho\pi}{5m}\left(2RZ - Z^2\right)^{3/2}} \tag{B5}$$

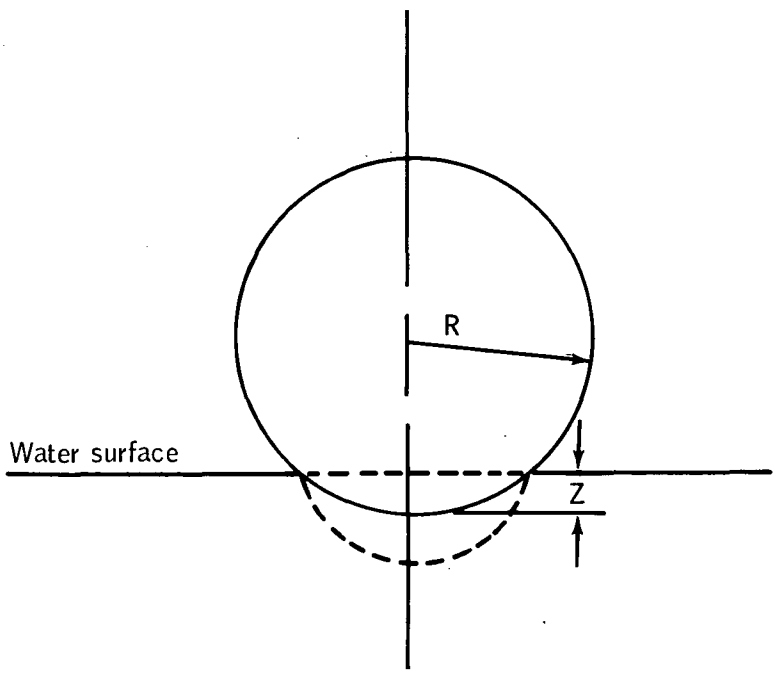

Figure B-1. - Geometry of sphere at water impact.

REFERENCES

1. Stubbs, Sandy M.; and Hathaway, Melvin E.: Effects of Bottom-Structure Flexibility on Water Landing Loads of Apollo Spacecraft Models. NASA TN D-5108, 1969.

2. Hathaway, M. E.; McGehee, J. R.; and Vaughan, V. L., Jr.: Water-Landing Characteristics of a Reentry Capsule. NASA Memo 5-23-59L, 1959.

3. Connolly, T. F.; Dommasch, D. O.; and Sherby, S. S.: Airplane Aerodynamics. Pitman Publishing, 1961.

4. Stubbs, Sandy M.: Dynamic Model Investigation of Water Pressures and Accelerations Encountered During Landings of the Apollo Spacecraft. NASA TN D-3980, 1967.

NASA-Langley, 1969 —— 32 S-208

NATIONAL AERONAUTICS AND SPACE ADMINISTRATION
WASHINGTON, D. C. 20546

OFFICIAL BUSINESS

FIRST CLASS MAIL

POSTAGE AND FEES PAID
NATIONAL AERONAUTICS AND
SPACE ADMINISTRATION

POSTMASTER: If Undeliverable (Section 158 Postal Manual) Do Not Return

"The aeronautical and space activities of the United States shall be conducted so as to contribute . . . to the expansion of human knowledge of phenomena in the atmosphere and space. The Administration shall provide for the widest practicable and appropriate dissemination of information concerning its activities and the results thereof."

— NATIONAL AERONAUTICS AND SPACE ACT OF 1958

NASA SCIENTIFIC AND TECHNICAL PUBLICATIONS

TECHNICAL REPORTS: Scientific and technical information considered important, complete, and a lasting contribution to existing knowledge.

TECHNICAL NOTES: Information less broad in scope but nevertheless of importance as a contribution to existing knowledge.

TECHNICAL MEMORANDUMS: Information receiving limited distribution because of preliminary data, security classification, or other reasons.

CONTRACTOR REPORTS: Scientific and technical information generated under a NASA contract or grant and considered an important contribution to existing knowledge.

TECHNICAL TRANSLATIONS: Information published in a foreign language considered to merit NASA distribution in English.

SPECIAL PUBLICATIONS: Information derived from or of value to NASA activities. Publications include conference proceedings, monographs, data compilations, handbooks, sourcebooks, and special bibliographies.

TECHNOLOGY UTILIZATION PUBLICATIONS: Information on technology used by NASA that may be of particular interest in commercial and other non-aerospace applications. Publications include Tech Briefs, Technology Utilization Reports and Notes, and Technology Surveys.

Details on the availability of these publications may be obtained from:

SCIENTIFIC AND TECHNICAL INFORMATION DIVISION

NATIONAL AERONAUTICS AND SPACE ADMINISTRATION

Washington, D.C. 20546